IEEE Access
Multidisciplinary | Rapid Review | Open Access Journal

Received September 16, 2019, accepted September 24, 2019, date of publication September 26, 2019,
date of current version October 29, 2019.

Digital Object Identifier 10.1109/ACCESS.2019.2944027

Removal of Power Line Interference From ECG Signals Using Adaptive Notch Filters of Sharp Resolution

BINQIANG CHEN[1], YANG LI[1], XINCHENG CAO[1], WEIFANG SUN[2], AND WANGPENG HE[3], (Member, IEEE)

[1]School of Aerospace Engineering, Xiamen University, Xiamen 361005, China
[2]College of Mechanical and Electrical Engineering, Wenzhou University, Wenzhou 325035, China
[3]School of Aerospace Science and Technology, Xidian University, Xi'an 710054, China

Corresponding author: Weifang Sun (vincent_suen@126.com)

This work was supported in part by the National Natural Science Foundation of China under Grant 51605403, in part by the Natural Science Foundation of Guangdong Province, China, under Grant 2015A030310010, in part by the Natural Science Foundation of Fujian Province, China, under Grant 2016J01012, in part by the Aeronautical Science Foundation of China under Grant 20183368004, and in part by the Fundamental Research Funds for the Central Universities under Grant 20720190009.

ABSTRACT The noise cancellation in electrocardiogram (ECG) signal is very influential to distinguish the essential signal features masked by noises. The power line interference (PLI) is the main source of noise in most of bio-electric signals. Digital notch filters can be used to suppress the PLI in ECG signals. However, the problems of transient interferences and the ringing effect occur, especially when the digitization of PLI does not meet the condition of full period sampling. In this paper, to obtain a better cancellation of the PLI, a designing approach, generating adaptive notch filter (ANF) of sharp resolution, is proposed. The proposed method is concise in algorithm and achieves a more comprehensive reduction of the PLI. It only requires on one fast Fourier transform on the input signal. The spectrum correction method, based on the information from the FFT spectrum of the corrupted signal, is utilized to estimate the harmonic parameters of the PLI. The information of a few main lobe spectral bins in the FFT spectrum is merged such that a compensation signal can be synthesized. By subtracting the compensational signal from the original measurement, the PLI within the investigated signal can substantially reduced. A distinguished advantage of the proposed ANF lies in the fact that no parameters are required to be specified, making the algorithm easier to be implemented. The proposed ANF outperforms conventional notch filters because it not only alleviates the undesirable effects but also better preserves the QRS-complex features in the filtered signal.

INDEX TERMS Electrocardiogram (ECG), power line interference, spectrum correction, adaptive notch filter.

I. INTRODUCTION

The measurement of the electrical activity of the heart is referred to as an electrocardiogram (ECG) [1], [2]. The reliable and accurate feature measurement of ECG signals plays an important role for the effective diagnosis of cardiovascular disease [3]–[5]. However, during the process of the ECG measurement, power line interference (PLI), which is of 50Hz in frequency, emerges as a major source of interference that significantly deteriorates signal quality if it is left untreated [6], [7].

To retrieve the actual ECG signal and to extract more accurate information for further analysis, the cancellation of PLI is necessary and thus attracts extensive attentions [8]–[10]. Many advanced signal processing techniques, which can remove the PLI from noisy ECG signals, have been reported in the literature [11]. Notch filter based methodologies, based on the classical theory of Fourier analysis, have found many applications. Either finite impulse response filters or infinite impulse response filters can be designed for this purpose. Piskorowski utilized multiple notch filtering

The associate editor coordinating the review of this manuscript and approving it for publication was Yongtao Hao.

methods to suppress harmonic power line interferences in ECG signals [12]. Vallejo proposed a spectro-temporal filtering technique for electrocardiogram enhancement and found a gain in signal-to-noise ratio improvement [13]. Wang put forward a novel design method to realize adaptive notch filters with infinite-impulse response such that harmonics in the signal can be removed [14].

Time-scale analysis (TSA) is also utilized in PLI cancellation and noise reduction of biological signals [15], [16]. TSA methods can be regarded as filterbank based techniques, which consist of a set of digital band-pass filters [17]–[19]. There are studies reporting the usage of the wavelet transform and the empirical mode decomposition for suppressing PLI. Liu investigated the time, second-order difference, and wavelet domain as sparse domains for the ECG signal and the frequency domain as the sparse domain for PLI [6]. Suchetha conducted a comparative analysis of EMD based filtering methods for 50 Hz noise cancellation in ECG signal [20]. Yadav proposed a novel non-local wavelet transform method for ECG signal denoising by exploiting the local and non-local redundancy present in the signal [21]. Sayed introduced an effective hybrid scheme for the denoising of ECG signals corrupted by non-stationary noises using genetic algorithm and wavelet transform [22].

Besides the above methodologies, other advanced methods, such as least mean square based adaptive filtering [23], adaptive Fourier transform [24], Kalman Filter [25], nonlinear Bayesian filtering [26], eigen-value decomposition [11], have also been investigated for the purpose of ECG denoising. Recently, artificial intelligence based techniques are also introduced to enable intelligent analysis of equipment monitoring signals and biomedical signals with noises [27]–[29]. Wang proposed an adversarial method for ECG signals de-noising and achieved up to about 62% improvement on the SNR of de-noised signals on average compared with state-of-the-art technologies [30]. Huang investigated the classification of ECG signals using the combination of short time Fourier transform and convolutional neural network [31]. Wang proposed a fast and accurate ECG classification system based on deep learning [32].

The problem of PLI removal in ECG signal analysis can be interpreted as the reduction of sinusoidal waves at some specific frequencies. We proposed a novel adaptive notch filter for PLI cancellation. The core of the proposed algorithm is the ratio based spectrum correction (RBSC). In the procedure, only one fast Fourier transform is required to be performed on the original ECG signal. A pair of spectral bins located within the main lobe of the Fourier spectrum can be used to estimate the amplitude, the frequency and the initial phase of the PLI such that a compensation signal can be constructed. By subtracting the compensation signal from the original ECG signal, the PLI can be effectively suppressed.

Two performances of two window based RBSC are compared and the Hanning window is chosen to be used in the algorithm. Numerical results show that the proposed ANF is more effective in suppressing undesirable phenomenon of transient interference and the ringing effect, which widely exist in notch filter based ECG de-noising techniques. ECG measurements from the dataset released by MIT-BIH are used to test the proposed method in actual ECG analysis. The results show that the ANF not only can suppress the undesirable phenomena, but also produces less residual QRS-complex features, which outperforms the performances of two comparison notch filters.

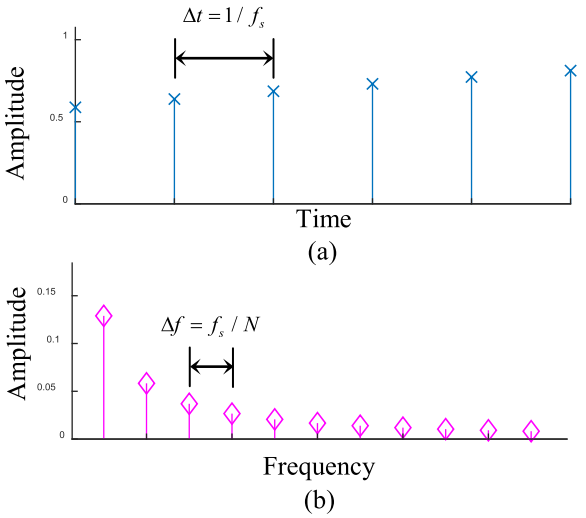

FIGURE 1. Relationship between (a) the digitized signal and (b) the associated FFT spectrum.

II. ENERGY LEAKAGE OF SINUSOIDAL WAVE IN DIGITAL SAMPLING

Usually in the digitization of a physical process, a time series of even spaced samples is recorded. In this section, we focus on explaining how the energy leakage problem occurs in spectrum based techniques. We will show that the condition of fully period sampling (FPS), which is determined by sampling parameters, has a substantial impact on the spectrum analysis of signals.

A. FUNDAMENTALS OF SPECTRUM ANALYSIS OF DIGITAL SIGNALS

Modern spectrum analysis relies heavily on the theory of discrete time Fourier Transform (DTFT). Cooley and Tukey developed the celebrated fast algorithm of fast Fourier transform (FFT), which decomposes a signal into the sum of a few sinusoidal waves. For a signal $x(t)$ sampled at the frequency f_s and the length N, the associated FFT spectrum $\hat{x}(k)$ is a complex valued series spaced at a uniform spatial interval of f_s/N in the frequency domain.

$$\hat{x}(k) = \sum_{n=0}^{N-1} x(n) e^{-j\frac{2\pi nk}{N}}, \tag{1}$$

where the constant j indicates the imaginary number and $k = 0, 1, \cdots, N-1$. The relationship between the sampling of $x(n)$ and that of $\hat{x}(k)$ is shown in Figure 1.

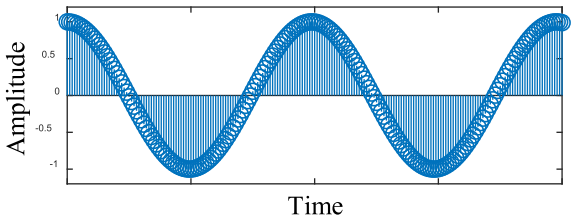

FIGURE 2. The waveform of an SHW in the time domain.

B. CONDITION OF FULL PERIOD SAMPLING FOR SIMPLE HARMONIC WAVE

A simple harmonic wave (SHW) is referred to as a dynamic process in which a sinusoidal wave of a specific frequency is included (Figure 2). The mathematical definition of a SHW can be defined as

$$shw(t) = A \cdot \cos(2\pi f_c t + \phi), \tag{2}$$

where A denotes the amplitude; f_c denotes the frequency of the SHW; and ϕ denotes the initial phase of the process. It can be inferred that an SHW, by nature, is a band limited signal of extremely narrow bandwidth (Figure 3(a)).

An SHW, of finite evenly spaced samples, is described to meet the demand of FPS if the following condition is satisfied.

$$N \cdot \frac{f_c}{f_s} \in \mathbb{N}^+, \tag{3}$$

where $\mathbb{N}^+$ denotes the set of positive integers. The Fourier spectrum of an SHW satisfying the FPS condition is a discrete Dirac sequence in the frequency domain (Figure 3(b), denoted as

$$\widehat{shw}(f) = \delta(f - f_c) = \begin{cases} 1, & f = f_c \\ 0, & f \neq f_c, \end{cases} \tag{4}$$

Otherwise it will become a discretized version of a broadband signal whose shape is determined by the FFT of the windows function (Figure 3(c)). Two most commonly used types of window are the rectangular window and the Hanning window.

C. NEGATIVE EFFECT CAUSED BY NON-FPS CONDITION

In the case of non-FPS condition, the energy leakage occurs across the entire frequency axis. A notch filter is designed in the frequency domain. As such, no matter what kind of notch filter is used, the FIR type or the FIR type, only a portion of the leakage components of PLI can be reduced. Owing to the incomplete reduction, an undesirable phenomenon of ringing effect is inevitable. The phenomenon is reflected as highly oscillated fluctuations of waveforms in the time domain. Although the amplitudes of the oscillations are not large, it still complicates subsequent processes of ECG analysis.

III. RATIO BASED SPECTRUM CORRECTION METHODS BASED ON RECTANGLE WINDOW AND HANNING WINDOW

A window function is often used in spectrum analysis because it is beneficial to suppress the energy leakage problem. RBSC

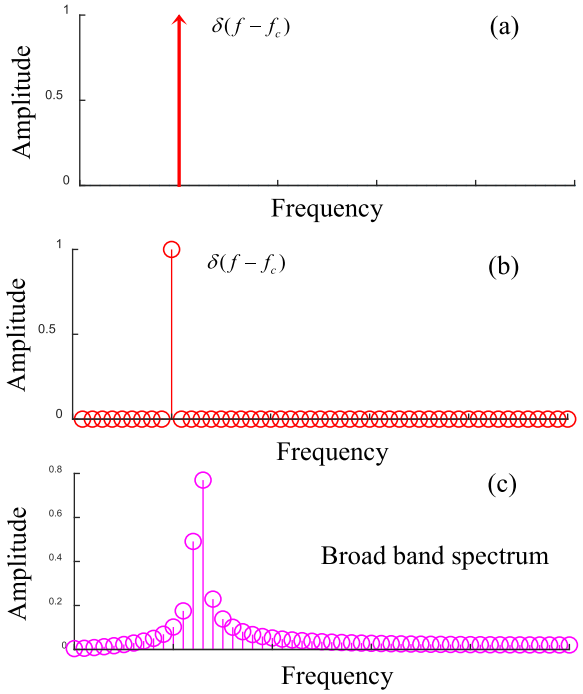

FIGURE 3. (a) The actual spectrum of an SHW; (b) the narrow band spectrum of an SHW when it satisfy the FPS condition; and (c) the broad band spectrum of an SHW when it does not satisfy the FPS condition.

can be interpreted as a preprocessing of the FFT spectra. More accurate harmonic information of A_c, f_c and ϕ_c can be estimated using a few main lobe spectral bins (MLSBs) located within the main lobe of a window function in the frequency domain.

A. SPECTRUM CORRECTION USING RECTANGLE WINDOW

The mathematical definition and the frequency response of a rectangle window is shown in Equation (5,6).

$$W_r(n) = 1 \quad for\ n = 1, 2, \ldots, N, \tag{5}$$

$$\hat{W}_r(w) = \frac{\sin(Lw/2)}{\sin(w/2)} e^{j(N-1)w/2}, \tag{6}$$

The window has the same length as that of the input signal. The modulus function of the frequency response is

$$T(k) = \frac{\sin(\pi k)}{\sin(\pi k/L)} \approx \frac{L \sin(\pi k)}{\pi k}, \tag{7}$$

and the shape of $T(k)$ is plotted in Figure 4(a). In the main lobe of the function, two MLSBs are utilized (Figure 4(b)). They are denoted as $T(\tilde{k})$ and $T(\tilde{k}+1)$.

Let the normalized error $\Delta k = k' - k$, where k' is the index of the window vertex associated with the actual spectral bin. This error can be computed as

$$\Delta k = -\frac{1}{1+v} = -\frac{T(\tilde{k}+1)}{T(\tilde{k}) + T(\tilde{k}+1)}, \tag{8}$$

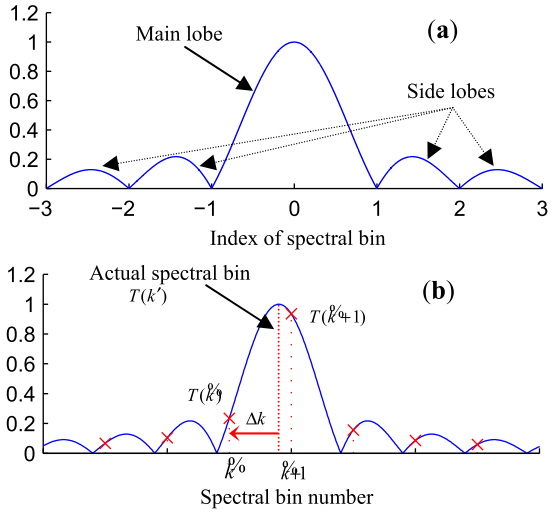

FIGURE 4. (a) The frequency response of a rectangle window; and (b) the MLSBs for spectrum correction.

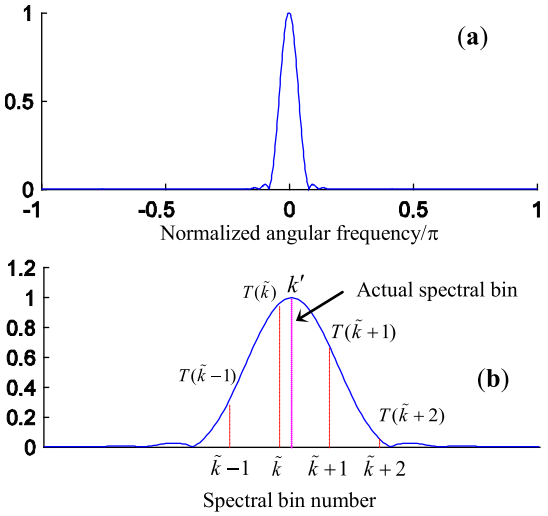

FIGURE 5. (a) The frequency response of a Hanning window; and (b) the MLSBs for spectrum correction.

where $v = T(\tilde{k})/T(\tilde{k}+1)$. Finally, the harmonic information of an SHW can be obtained as below.

$$\begin{cases} A_c = \dfrac{\pi \Delta k \cdot T(k)}{\sin(\pi \Delta k)} \\ f_c = (k + \Delta k)\dfrac{f_s}{L} \\ \phi_c = \arctan \dfrac{Im(k')}{Re(k')} - \pi \Delta k, \end{cases} \tag{9}$$

B. SPECTRUM CORRECTION USING HANNING WINDOW

The mathematical definition and the frequency response of a Hanning window is shown in Equation (10,11).

$$W_h(n) = \frac{1}{2} - \frac{1}{2}\cos\left(\frac{2\pi n}{L}\right) \quad for\ n = 0, 1, 2 \ldots, L-1, \tag{10}$$

$$\hat{W}_h(w) = \left\{\frac{1}{2}\hat{W}_r(w) + \frac{1}{4}\left[\hat{W}_r\left(w - \frac{2\pi}{L}\right) + \hat{W}_r\left(w + \frac{2\pi}{L}\right)\right]\right\} e^{-jNw/2}, \tag{11}$$

The modulus function of the frequency response is

$$T(k) = \frac{\sin(\pi k)}{2\pi k} \cdot \frac{1}{1-k^2}, \tag{12}$$

and the shape of $T(k)$ is plotted in Figure 5(a). When the FPS condition is not satisfied, there are four MLSBs existed in the main lobe. However, only the two with larger amplitudes are selected (Figure 5(b)). The error between k', the index of the actual spectral bin, and $\tilde{k}$, is calculated used the following equation

$$\Delta k = \frac{v-2}{v+1}, \tag{13}$$

where the $v = T(\tilde{k})/T(\tilde{k}+1)$. Finally the harmonic information of an SHW can be estimated as

$$\begin{cases} A_c = \dfrac{\pi \Delta k \cdot T(\tilde{k})}{\sin(\pi \Delta k)} \cdot 2[1 - (\Delta k)^2] \\ f_c = (k + \Delta k)\dfrac{f_s}{L} \\ \phi_c = \arctan \dfrac{Im(k')}{Re(k')} - \pi \Delta k, \end{cases} \tag{14}$$

IV. DESIGN OF ADAPTIVE NOTCH FILTER OF SHARP RESOLUTION BASED ON RBSC

If the frequency of the PLI is exactly 50Hz, it is feasible to avoid energy leakage by properly selecting the sampling parameters. However, the value of the actual frequency is just approximately 50. An error of the power frequency in the range of [−2, 2]Hz can be found according to power quality control regulations, for example in China. RBSC based techniques can be employed to design adaptive notch filter of extremely sharp resolution. The procedure of the proposed methodology is stated as below.

Step 1). Let the analyzed signal be $ecg(t)$ of sampling frequency f_s and length N. Perform the fast Fourier transform on the signal $ecg(t)$.

$$ecg(t) \xrightarrow{FFT} \widehat{ecg}(f)$$

Step 2). Search two spectral bins of large amplitudes within the main lobe of the PLI in the frequency domain. Estimate the harmonic information ($A_{\mathrm{PLI}}, f_{\mathrm{PLI}}$ and ϕ_{PLI}) of the PLI by ratio based spectrum correction methods.

$$\widehat{ecg}(f) \xrightarrow{RBSC} A_{\mathrm{PLI}}, f_{\mathrm{PLI}}, \phi_{\mathrm{PLI}}$$

Step 3). Construct a compensation signal $comp_{\mathrm{PLI}}(t)$ based on the extracted harmonic information.

$$comp_{\mathrm{PLI}}(t) = A_{\mathrm{PLI}} \cdot \cos(2\pi f_{\mathrm{PLI}} t + \phi_{\mathrm{PLI}})$$

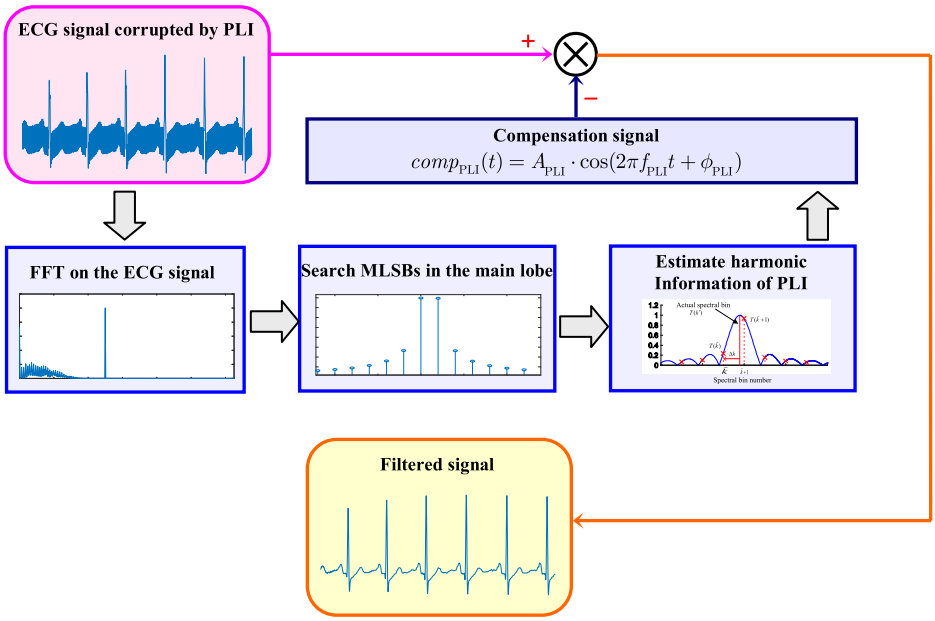

FIGURE 6. Flow chart of the algorithm of the adaptive notch filter.

Step 4) Subtract $comp_{\mathrm{PLI}}(t)$ from the corrupted ECG signal.

$$\overline{ecg}(t) = ecg(t) - comp_{\mathrm{PLI}}(t)$$

The algorithm belongs to the type of parameter free. A flow chart of the proposed algorithm is displayed as in Figure 6.

V. COMPARISON OF PERFORMANCES OF TWO SPECTRUM CORRECTION METHOS

Either of the two windows can be employed to estimate the harmonic frequency of PLI in ECG signals. In this section, we test the estimation performance of the RBSCs with the two types of windows.

A. COMPARISON OF PERFORMANCE FOR NOISE-FREE SHW

In this subsection, a digital signal $x(t)$ containing one SHW is simulated.

$$x_c(t) = A_c \cos(2\pi f_c t + \phi_c), \tag{15}$$

where the amplitude A_c is chosen as 1 without loss of generality. The sampling length of celebrated datasets of ECG measurement are mainly 200∼400Hz. Therefore, we set the sampling frequency of $x(t)$ as 1, and 250 digital samples are utilized in the following comparison.

To simulate the error of power line frequency, the parameter f_c is set as

$$f_c = 50 + \Delta f, \tag{16}$$

Supposing that $y_{rec}(t)$ and $y_{han}(t)$ are synthesized signals reconstructed using the rectangular window based RBSC and the Hanning window based RBSC, respectively, the reconstruction errors between $x(t)$ and the synthesized signals

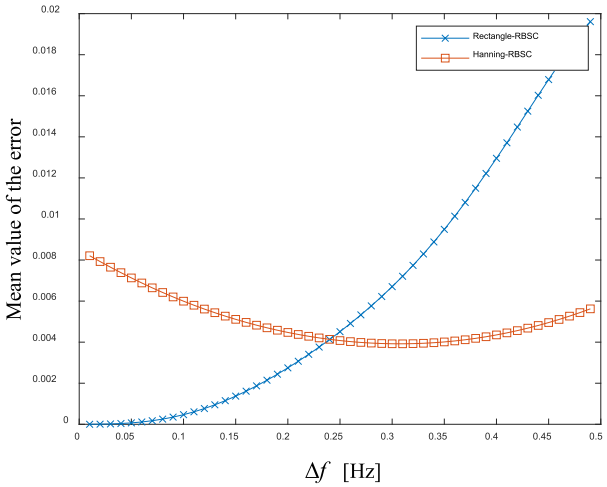

FIGURE 7. (a) The frequency response of a Hanning window; and (b) the MLSBs for spectrum correction.

using the following formulae.

$$err_{rec} = \|y_{rec}(t) - x(t)\|_2^2, \tag{17}$$

$$err_{rec} = \|y_{rec}(t) - x(t)\|_2^2, \tag{18}$$

where $||\ \cdot\ ||_2$ means to compute the 2-norm of input series.

Let the frequency error be ranged in the interval of [0, 0.5]Hz, the reconstruction errors of the two RBSC methods are shown in Figure 7. It can be seen that when $\Delta f \in [0, 0.25]Hz$, the rectangular window based RBSC has better performance. While when $\Delta f \in [0.25,\ 0.5]Hz$, the Hanning window based RBSC has better performance. No matter what kind of window is used, the reconstruction error is small and acceptable for high precision estimation.

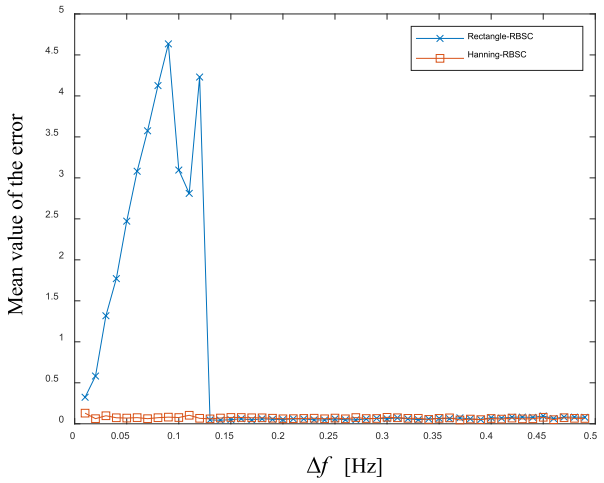

FIGURE 8. (a) The frequency response of a Hanning window; and (b) the MLSBs for spectrum correction.

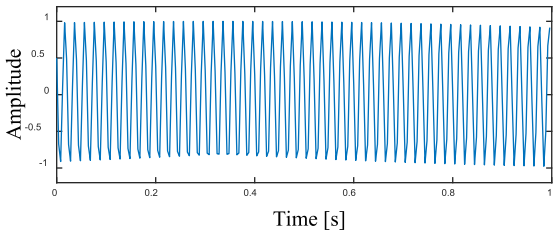

FIGURE 9. The waveform of the simulated simple harmonic wave.

B. COMPARISON OF PERFORMANCE FOR SHW CORRUPTED BY GAUSSIAN NOISES

In this subsection, we create a noisy version of the signal $x_c(t)$ as

$$\tilde{x}_c(t) = x_c(t) + wgn(t). \tag{19}$$

The same sampling parameters are adopted as those in $x_c(t)$. The signal-to-noise ratio of the noisy signal is set as 20. The resulting reconstruction errors using the two types of windows are shown in Figure 8. For all values of Δf, the curves of the reconstruction errors based on Hanning window RBSC is stable. While for the case of rectangle window, large errors are produced when $\Delta f \in [0.01,\ 0.13]$. This phenomenon is caused by one MLSB small in amplitude.

C. RESULT ANALYSIS

The actual ECG measurement is not free of noise. As shown in the comparisons, the Hanning windows based RBSC is more robust in correction harmonic information of SHW not satisfying FPS condition. Therefore, we choose the type of window, which is utilized in the algorithm of Section IV, as the Hanning window.

VI. COMPARISON OF THE PROPOSED METHOD WITH CONVENTIONAL NOTCH FITLER IN REDUCTION OF SHW

Following the definition in Equation (15), an SHW with frequency is 50.1Hz is simulated and the waveform is shown in Figure 9.

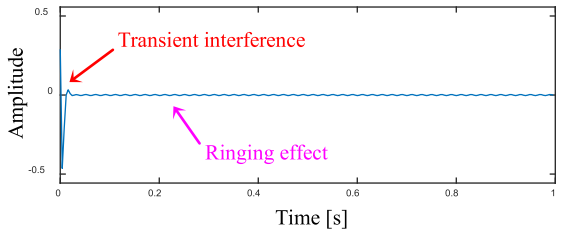

FIGURE 10. The waveform of the simulated simple harmonic wave.

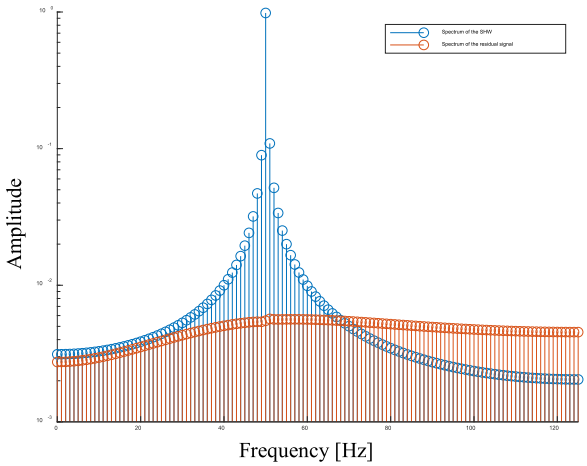

FIGURE 11. The Fourier spectra of the simulated signal and the filtered signal by the IIR notch filter.

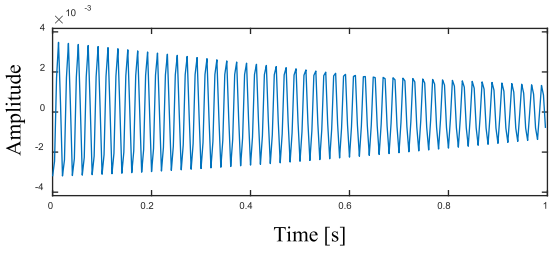

FIGURE 12. The waveform of the filtered signal using the proposed method.

An IIR notch filter is constructed to remove the SHW. The central frequency and the bandwidth of the notch filter are set as 50Hz and 0.4Hz. The filter result is shown in Figure 10. Undesirable phenomena of the transient interference at the beginning samples and the ringing effect can be easily recognized in Figure 11.

The Fourier spectra of the simulated signal and the filtered signal are shown in Figure 11. The scale of Y-axis this figure is set as in the mode of logarithm. The leakage components, whose frequencies are closed to 50Hz, are effectively reduced; however spectral bins with larger distances from the central frequency of the notch filter are preserved. This leads to the undesirable phenomena of filtering based on the IIR filter.

Figure 12 shows the filtering result using the proposed method. The maximal absolute value of the signal is smaller

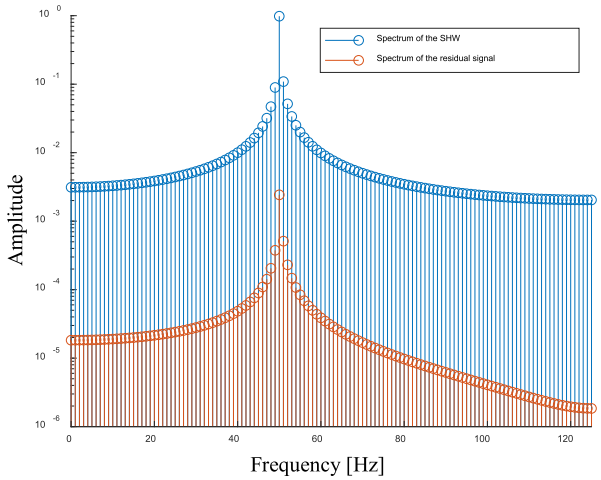

FIGURE 13. The Fourier spectra of the simulated signal and the filtered signal by the proposed method.

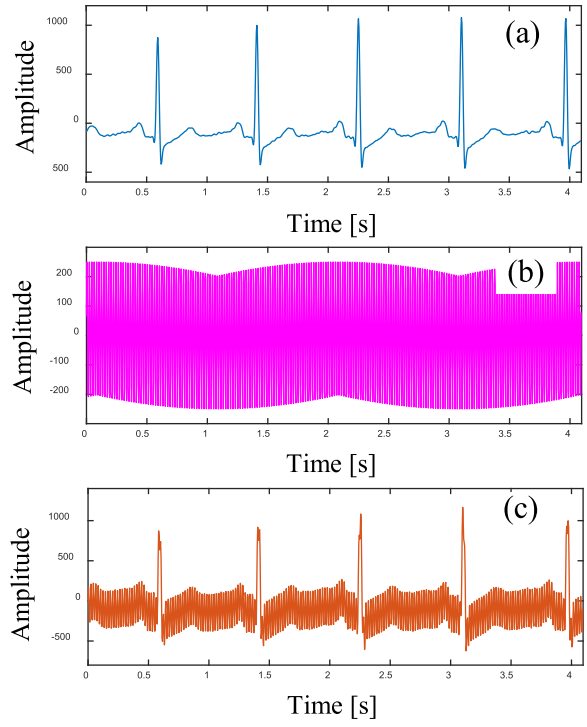

FIGURE 14. (a) The waveform of the original ECG signal; (b) the simulated PLI; and (c) the simulated ECG signal with PLI.

than 4×10^{-3}. Although the ringing effect still exists, it can be neglected due to extremely small amplitudes. The root-mean-square values of the ringing parts of the two filtered signals in Figure 10 and Figure 12 are 0.024 and 0.016 respectively, which demonstrates the enhancement of the proposed method in the suppression of the ringing effect.

Figure 13 shows the Fourier spectra of the simulated signal and the filtered result by the proposed method. The amplitudes of the leakage components across the entire frequency axis are substantially reduced.

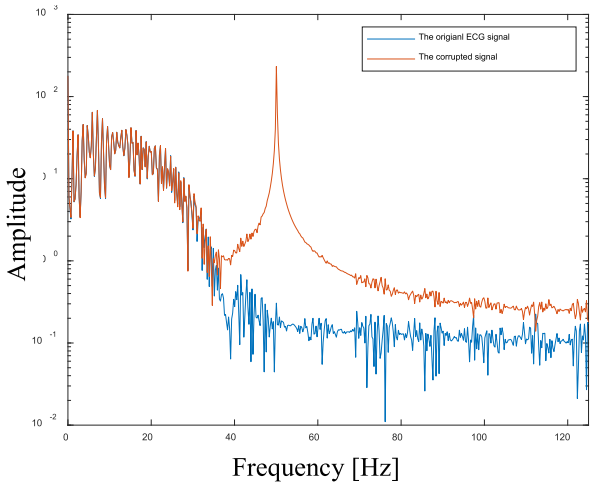

FIGURE 15. The Fourier spectra of the original ECG signal and the simulated signal corrupted by PLI.

VII. NUMERICAL ANALYSIS OF THE PROPOSED METHOD IN ECG SIGNALS

To evaluate the performance of the proposed method in processing ECG signals corrupted by PLI, measurements of ECG form the dataset of MIT-BIH polysomnographic database (http://www.physionet.org/cgi-bin/atm/ATM) are utilized. In this section, the original ECG signal to be analyzed is denoted as $d(n)$. The sampling frequency and the sampling length of the signal is 250 and 1024.

An SHW is simulated to be the PLI of the original ECG signal. The harmonic information of the SHW are

$$\begin{cases} A_c = 250 \\ f_c = 50.1\text{Hz} \\ \phi_c = 15°. \end{cases} \tag{20}$$

The waveform of the simulated PLI is shown in Figure 14(b). By summing the original ECG signal and the SHW, the simulated signal with PLi is shown in Figure 14(c). The SNR of the simulated signal is 1dB. The Fourier spectra of the original ECG signal and the simulated signal are shown in Figure 15.

Based on the proposed ADF method, the filter signal and reconstruction errors are shown in Figure 16. The construction error is pretty small. The largest value of the errors is smaller than 1.5.

The comparison between the Fourier spectrum of the original ECG signal and that of the filtered signal is shown in Figure 17. It can be seen, the two signals are very similar except for a few spectral bins round the neighborhood of the actual frequency of the PLI.

We utilized two types of IIR notch filter to process the signal. One is the conventional IIR filter employed in Section VI. The filtered signal and its Fourier spectrum are shown in Figure 18. Although the waveform of the filtered signal is very similar to the original ECG signal. The curve of errors between the two signals reveals that phase shift is produced

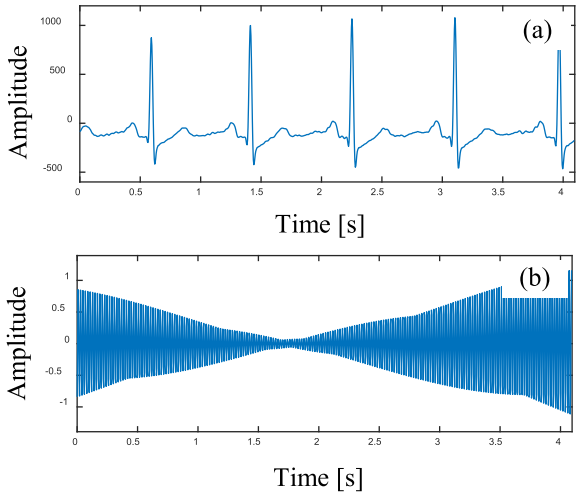

FIGURE 16. (a) The filtered signal using the proposed method; and (b) the construction errors between the filtered signal and the original ECG signal.

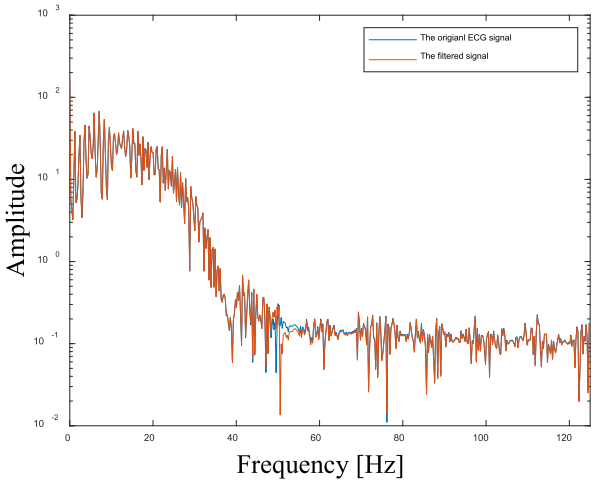

FIGURE 17. Comparison between the original ECG signal and filtered signal.

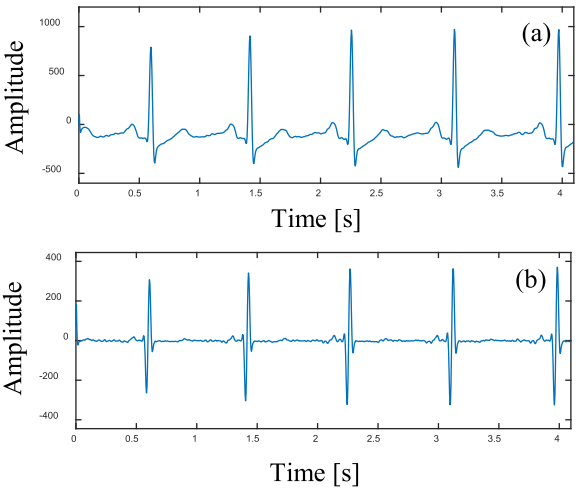

FIGURE 18. (a) The filtered signal using the conventional IIR filter; and (b) the construction errors between the filtered signal and the original ECG signal.

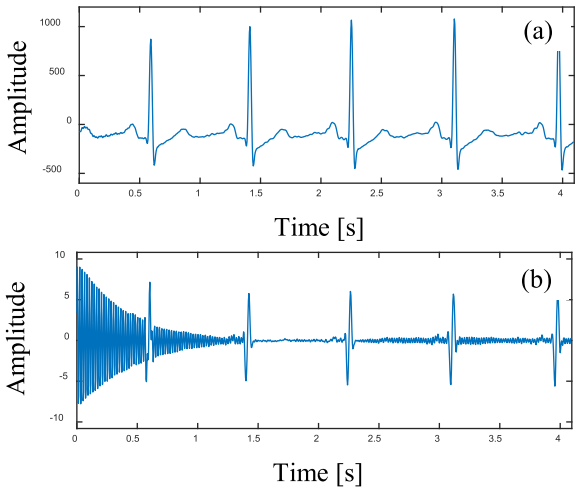

FIGURE 19. (a) The filtered signal using the improved IIR filter; and (b) the construction errors between the filtered signal and the original ECG signal.

in the IIR filtering process and causes very large errors in the neighboring areas of the impulsive QRS-complex features. The maximal error can be as high as 300. On the other hand, transient interferences are also detected at some beginning samples of the filtered signal.

The other comparison method is an improved IIR with transient interference suppression ability [10]. The filtered result and the construction error are shown in Figure 19. In Figure 19(b), the transient interferences at the beginning samples and the residual QRS-complex features are much smaller than those in Figure 18(b).

Comparisons between the waveform of the original ECG signal and those of the filtered signal generated by the two comparison IIR notch filters are shown in Figure 20. In Figure 20(a), relatively large errors are found in the high frequency range of the proposed method. To make a more quantitative analysis, the maximal value and the RMS value of the construction errors are computed. The related information is shown in Table 1. The construction error by the proposed method is the smallest in the indicators of maximal error and RMS of errors. These comparisons have validated that the proposed ANF outperforms traditional IIR notch filter based techniques.

TABLE 1. Comparisons between the proposed method and two types of IIR notch filters.

	The proposed method	The conventional IIR filter		The improved IIR filter	
		Entire signal	Ringing part	Entire signal	Ringing part
Maximal error	1.1601	9.0063	6.0187	370.58	370.58
RMS of errors	0.4436	1.8412	1.0015	60.7558	60.9910

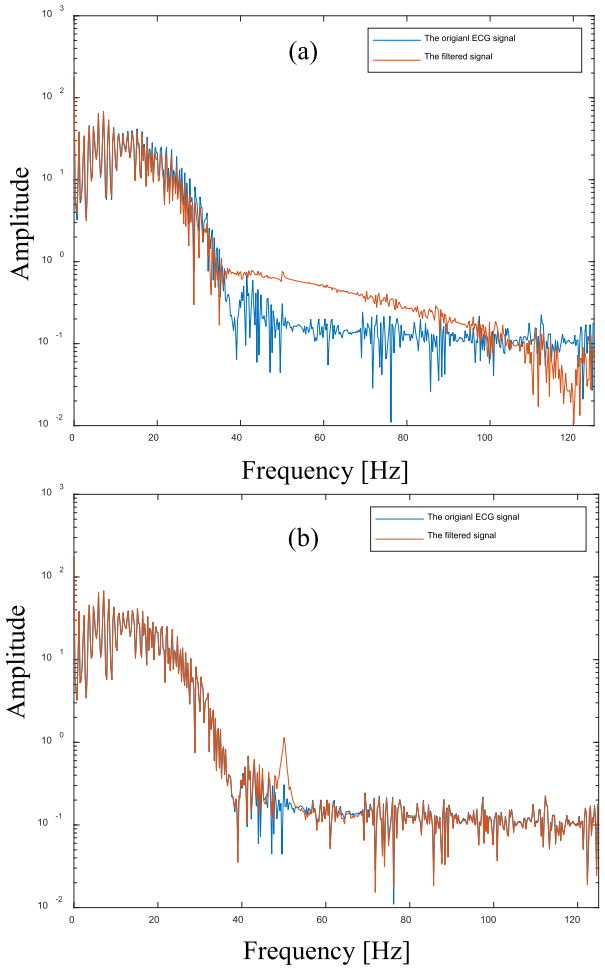

FIGURE 20. **(a) The filtered signal using the conventional IIR filter; and (b) the construction errors between the filtered signal and the original ECG signal.**

VIII. CONCLUSION

The findings the paper are summarized as below.

(1) The PLI emerges in the form of simple harmonic wave. The phenomenon of energy leakage occurs when the sampling of the PLI does not meet the condition of FPS. In such situations, conventional notch filters can not suppress all spectral bins related to energy leakage, which causes undesirable effects in the filtered signal.

(2) A novel adaptive notch filter based on RBSC is proposed in this paper. In noisy measurements, the Hanning window based RBSC is more robust in acquiring high precision harmonic information. In simulations of SHW reduction, the proposed method was compared with a conventional IIR notch filter. Results show that the proposed ANF of sharp resolution can better suppress the ringing effect and causes no transient interferences at the beginning samples of the filtered signal.

(3) The ECG measurements form the dataset released by MIT-BIH are used for test the performance of the proposed method. An additive 50Hz PLI is added to the original ECG signal to simulate ECG signals corrupted by PLI. The proposedi method is compared with two IIR notch filters. It is found that the maximal value and the RMS value of construction errors, produced by the proposed ANF, are smallest among the results of three methods, indicating an improved SNR in the filtered signal.

REFERENCES

[1] E. N. Bruce, *Biomedical Signal Processing and Signal Modeling*. New York, NY, USA: Wiley, 2001.

[2] P. E. McSharry, G. D. Clifford, L. Tarassenko, and L. A. Smith, "A dynamical model for generating synthetic electrocardiogram signals," *IEEE Trans. Biomed. Eng.*, vol. 50, no. 3, pp. 289–294, Mar. 2003.

[3] K. Friganovic, D. Kukolja, A. Jovic, M. Cifrek, and G. Krstacic, "Optimizing the detection of characteristic waves in ECG based on processing methods combinations," *IEEE Access*, vol. 6, pp. 50609–50626, 2018.

[4] N. Vemishetty, P. Patra, P. K. Jha, K. B. Chivukula, C. K. Vala, A. Jagirdar, V. Y. Gudur, A. Acharyya, and A. Dutta, "Low power personalized ECG based system design methodology for remote cardiac health monitoring," *IEEE Access*, vol. 4, pp. 8407–8417, 2016.

[5] O. Yildirim, T. R. San, and U. R. Acharya, "An efficient compression of ECG signals using deep convolutional autoencoders," *Cognit. Syst. Res.*, vol. 52, pp. 198–211, Dec. 2018.

[6] H. Liu, Y. Li, Y. Zhou, X. Jing, and T.-K. Truong, "Joint power line interference suppression and ECG signal recovery in transform domains," *Biomed. Signal Process. Control*, vol. 44, pp. 58–66, Jul. 2018.

[7] Y.-D. Lin and Y. H. Hu, "Power-line interference detection and suppression in ECG signal processing," *IEEE Trans. Biomed. Eng.*, vol. 55, no. 1, pp. 354–357, Jan. 2008.

[8] C. Chandrakar and M. K. Kowar, "Denoising ECG signals using adaptive filter algorithm," *Int. J. Soft Comput. Eng.*, vol. 2, no. 1, pp. 120–123, Mar. 2012.

[9] J. Glover, "Adaptive noise canceling applied to sinusoidal interferences," *IEEE Trans. Acoust., Speech, Signal Process.*, vol. 25, no. 6, pp. 484–491, Dec. 1977.

[10] S.-C. Pei and C.-C. Tseng, "Elimination of AC interference in electrocardiogram using IIR notch filter with transient suppression," *IEEE Trans. Biomed. Eng.*, vol. 42, no. 11, pp. 1128–1132, Nov. 1995.

[11] R. R. Sharma and R. B. Pachori, "Baseline wander and power line interference removal from ECG signals using eigenvalue decomposition," *Biomed. Signal Process. Control*, vol. 45, pp. 33–49, Aug. 2018.

[12] J. Piskorowski, "Suppressing harmonic powerline interference using multiple-notch filtering methods with improved transient behavior," *Measurement*, vol. 45, no. 6, pp. 1350–1361, Jul. 2012.

[13] D. P. Tobón and T. H. Falk, "Adaptive spectro-temporal filtering for electrocardiogram signal enhancement," *IEEE J. Biomed. Health Inform.*, vol. 22, no. 2, pp. 421–428, Mar. 2018.

[14] Q. Wang, X. Gua, and J. Lin, "Adaptive notch filter design under multiple identical bandwidths," *AEU-Int. J. Electron. Commun.*, vol. 82, pp. 202–210, Dec. 2017.

[15] M. Suchetha and N. Kumaravel, "Empirical mode decomposition based filtering techniques for power line interference reduction in electrocardiogram using various adaptive structures and subtraction methods," *Biomed. Signal Process. Control*, vol. 8, pp. 575–585, Nov. 2013.

[16] S. Poornachandra, "Wavelet-based denoising using subband dependent threshold for ECG signals," *Digit. Signal Process.*, vol. 18, no. 1, pp. 49–55, Jan. 2008.

[17] N. U. Rehman and D. P. Mandic, "Filter bank property of multivariate empirical mode decomposition," *IEEE Trans. Signal Process.*, vol. 59, no. 5, pp. 2421–2426, May 2011.

[18] B. Chen, Z. Zhang, Y. Zi, Z. He, and C. Sun, "Detecting of transient vibration signatures using an improved fast spatial-spectral ensemble kurtosis kurtogram and its applications to mechanical signature analysis of short duration data from rotating machinery," *Mech. Syst. Signal Process.*, vol. 40, no. 1, pp. 1–37, 2013.

[19] Y. Liu, Y. Li, H. Lin, and H. Ma, "An amplitude-preserved time—Frequency peak filtering based on empirical mode decomposition for seismic random noise reduction," *IEEE Geosci. Remote Sens. Lett.*, vol. 11, no. 5, pp. 896–900, May 2014.

[20] M. Suchetha, N. Kumaravel, M. Jagannath, and S. K. Jaganathan, "A comparative analysis of EMD based filtering methods for 50 Hz noise cancellation in ECG signal," *Inform. Med. Unlocked*, vol. 8, pp. 54–59, 2017.

[21] S. K. Yadav, R. Sinha, and P. K. Bora, "Electrocardiogram signal denoising using non-local wavelet transform domain filtering," *IET Signal Process.*, vol. 9, no. 1, pp. 88–96, Feb. 2015.
[22] E.-S. A. El-Dahshan, "Genetic algorithm and wavelet hybrid scheme for ECG signal denoising," *Telecommun. Syst.*, vol. 46, no. 3, pp. 209–215, Mar. 2011.
[23] F. Xiong, D. Y. Chen, Z. H. Chen, and S. M. Dai, "Cancellation of motion artifacts in ambulatory ECG signals using TD-LMS adaptive filtering techniques," *J. Vis. Commun. Image Represent.*, vol. 58, pp. 606–618, Jan. 2019.
[24] Z. Wang, F. Wan, C. M. Wong, and L. Zhang, "Adaptive Fourier decomposition based ECG denoising," *Comput. Biol. Med.*, vol. 77, pp. 195–205, Aug. 2016.
[25] N. Zeng, Z. Wang, Y. Li, M. Du, and X. Liu, "A hybrid EKF and switching PSO algorithm for joint state and parameter estimation of lateral flow immunoassay models," *IEEE/ACM Trans. Comput. Biol. Bioinf.*, vol. 9, no. 2, pp. 321–329, Mar./Apr. 2012.
[26] R. Sameni, M. B. Shamsollahi, C. Jutten, and G. D. Clifford, "A nonlinear Bayesian filtering framework for ECG denoising," *IEEE Trans. Biomed. Eng.*, vol. 54, no. 12, pp. 2172–2185, Dec. 2007.
[27] X.-C. Cao, B.-Q. Chen, B. Yao, and W.-P. He, "Combining translation-invariant wavelet frames and convolutional neural network for intelligent tool wear state identification," *Comput. Ind.*, vol. 106, pp. 71–84, Apr. 2019.
[28] X.-C. Cao, B. Yao, and B.-Q. Chen, "Atrial fibrillation detection using an improved multi-Scale decomposition enhanced residual convolutional neural network," *IEEE Access*, vol. 7, pp. 89152–89161, 2019.
[29] N. Zeng, Z. Wang, B. Zineddin, Y. Li, M. Du, L. Xiao, X. Liu, and T. Young, "Image-based quantitative analysis of gold immunochromatographic strip via cellular neural network approach," *IEEE Trans. Med. Imag.*, vol. 33, no. 5, pp. 1129–1136, May 2014.
[30] J. Wang, R. Li, R. Li, K. Li, H. Zeng, G. Xie, and L. Liu, "Adversarial denoising of electrocardiogram," *Neurocomputing*, vol. 349, pp. 212–224, Jul. 2019.
[31] J. Huang, B. Chen, B. Yao, and W. He, "ECG arrhythmia classification using STFT-based spectrogram and convolutional neural network," *IEEE Access*, vol. 7, pp. 92871–92880, 2019.
[32] E. K. Wang, X. Zhang, and L. Pan, "Automatic classification of CAD ECG signals with SDAE and bidirectional long short-term term network," *IEEE Access*, vol. 7, p. 1, 2019.

BINQIANG CHEN was born in Fujian, China, in 1986. He received the bachelor's degree in mechanical engineering from the School of Manufacturing Science and Technology, Sichuan University, in 2008, and the Ph.D. degree in mechanical engineering from the School of Mechanical Engineering, Xi'an Jiaotong University, in 2013. His main research interests include intelligent equipment and smart manufacturing, structural health monitoring of equipment, and applied harmonic analysis.

YANG LI was born in Heze, Shandong, China, in 1994. She received the bachelor's degree in mechanical design manufacture and automation from the School of Electromechanical and Automotive Engineering, Yantai University, in 2017. She is currently pursuing the master's degree with the School of Aerospace Engineering, Xiamen University, China. Her main research interests include intelligent equipment and smart manufacturing, and structural health monitoring of equipment.

XINCHENG CAO was born in Weifang, Shandong, China, in 1992. He received the bachelor's and master's degrees in mechanical engineering from the School of Aerospace Engineering, Xiamen University, China, in 2015 and 2018, respectively, where he is currently pursuing the Ph.D. degree. His main research interests include intelligent equipment and smart manufacturing, and structural health monitoring of equipment.

WEIFANG SUN was born in Xiangyang, Hubei, China, in 1988. He received the M.S. degree from Huazhong Agricultural University, Wuhan, China, in 2014, and the Ph.D. degree from Xiamen university, Xiamen, China, in 2018. He is currently an Assistant Professor with the College of Mechanical and Electrical Engineering, Wenzhou University. His research interests include dynamic modeling and diagnosis of electromechanical systems, digital information analysis, and artificial intelligence method.

WANGPENG HE was born in Yulin, Shaanxi, China. He received the B.S. and Ph.D. degrees in mechanical engineering from Xi'an Jiaotong University, Xi'an, China, in 2007 and 2016, respectively. In 2014, he was appointed as a Visiting Scholar with New York University, USA. He joined the School of Aerospace Science and Technology, Xidian University, where he is currently an Assistant Professor. His research interests include signal processing, machine vision, sparsity-based signal processing, and machinery fault diagnosis.